Radiation damage calculations for charged particle emission nuclear reactions

Shengli Chen, David Bernard

Version of Record: https://www.sciencedirect.com/science/article/pii/S0577907320301295
Manuscript_d995c52b430b984f5dcf93669f7c8ed2

Radiation damage calculations for charged particle emission nuclear reactions

Shengli Chen[1,2,*], David Bernard[1]

[1] CEA, DES, IRESNE, DER, SPRC, LEPh, 13108 Saint-Paul-Lez-Durance, France
[2] Université Grenoble Alpes, I-MEP2, 38402 Saint Martin d'Hères, France

[*] Corresponding author: shengli.chen@cea.fr

Abstract

Taking the quantum tunneling and Coulomb barrier into account, the present work proposes the calculation of Primary Knock-on Atom (PKA) energy for charged particle emission reactions. The method proposed in this paper and that used in NJOY have a large difference of PKA energy for charged particle emissions. For a D+T fusion neutron-induced ^{6}Li(n,t)^{4}He PKA, the maximum PKA energy calculated with NJOY is 2.9 MeV, whereas 14.2 MeV is obtained with the formula proposed in the present work. The subsequent total neutron-induced Displacement per Atom (DPA) calculated with the two methods has a small difference for most isotopes of which the DPA is predominated by scattering reactions, such as ^{56}Fe and ^{58}Ni. However, the difference can be important for nuclei with charged particle emission channels open at thermal energy, such as ^{6}Li, ^{10}B, and ^{59}Ni. Using the damage cross sections (calculated by NJOY with and without modifications) and SRIM/TRIM-2008 calculations, the relative differences on total DPA rates of the compound material 90%^{56}Fe-9%^{58}Ni-1%^{59}Ni are within 1% for two fast spectra, 1.5% for fusion first wall, about 5% for the heavy reflector, and 25% for a pressurized water reactor vessel.

Keywords: Quantum tunneling, Coulomb barrier, PKA energy, Displacement per Atom (DPA), Polyatomic materials, SRIM calculation

1. Introduction

Due to the change of behaviors of materials under and after irradiation, the irradiation damage is a key factor for investigating the properties of nuclear materials. The irradiation damage is conventionally quantified by the Displacement per Atom (DPA) number of materials. To compute DPA, many models have been developed in the past decades, such as Binary Collision Approximation (BCA) [1], Molecular Dynamics (MD) simulations [2], *ab initio* calculations with Density Functional Theory (DFT) [3], and some general DPA formulae summarized or proposed in the Nuclear Energy Agency (NEA) report [4]. These models predict the number of DPA for a specific Primary Knock-on Atom (PKA) energy. Different simulation methods are discussed by Becquart *et al.* [5]. The first step of DPA calculations for nuclear reactors is to determine the PKA energies so that one can compute DPA using the

above methods.

To use a similar method of reaction rate calculations in reactor physics, the widely used method for DPA calculation is to determine the DPA cross sections [6]. The DPA rates can be calculated using DPA cross sections and the corresponding spectra of incident particles [7], such as neutron, photon, and proton. The DPA cross sections for electron, positron, and photon are summarized in Ref. [8], those for neutron are typically calculated with NJOY [6], the proton-induced DPA cross sections can be found in Ref. [9] for theoretical calculations and in Ref. [10] for experimental measurements. Ref. [11] shows the deuteron-induced DPA cross sections for iron and two stainless steels. The beta decay-induced DPA calculation is also investigated [12]. Few works are performed for DPA cross sections induced by particles with 3 and 4 nucleons. However, using the corresponding nuclear reaction data as given in JEFF-3.3 [13] or other nuclear data libraries, the DPA cross sections can be determined.

Because only the PKAs are considered in the calculations of DPA cross sections, current DPA cross sections are more like PKA cross sections. A recent work shows the importance of the ^{4}He-induced damage for boron carbide [14]. In fact, the atomic displacements induced by the emitted light particles can always be taken into account by using the current PKA cross sections and spectra of all light particles, i.e. electron, positron, photon, neutron, proton, deuteron, triton, ^{3}He, and ^{4}He. Comparing with the method that takes the emitted light particles into account in DPA cross sections of each nucleus, the use of PKA cross sections and spectra of these light particles can larger simplify the calculations. For example, rather than computing the DPA rates induced by protons via the (n,p) reaction of all nuclei, one can directly multiply the proton spectra determined by transport codes with the proton-induced PKA cross sections. Moreover, these light particles from radioactive decays can be also directly included in the corresponding spectra. Since the current PKA cross sections can be used to determine the total DPA rate in folding with incident spectra, the PKA cross section is still referred to the DPA cross section hereinafter.

The calculation of DPA cross sections is based on PKA energy and reaction cross sections. For charged particle emission nuclear reactions, the energy of the system should be larger than the Coulomb barrier. Classical mechanics implies that the nuclear reaction is impossible if the system has energy lower than the Coulomb barrier. However, in quantum mechanics, even if the system has energy below the Coulomb barrier before the reaction, the reaction is possible due to the quantum tunneling. The present work takes the quantum tunneling into account in the calculation of PKA energy and the subsequent DPA cross section.

The methods for computing PKA energies from charged particle emission reactions are presented in Section 2.1. Section 2.2 reviews the methods for the calculations of DPA cross sections for pure isotopes. Based on the definition of DPA cross sections, Section 2.3 shows the calculation of DPA cross sections for compound materials. The direct relationship between DPA cross sections of polyatomic materials and those of pure atoms is found with two additional hypotheses. Section 2.4 illustrates the two methods for computing the DPA rate using incident spectra in

applications. Due to the important role of neutron in nuclear reactors, the studies on neutron-induced irradiation damage are necessary. Section 3 shows the results for PKA energies, DPA cross sections, and DPA rates in different nuclear facilities for neutron-induced charged particle emission reactions. The main conclusions are summarized in Section 4.

2. Methods

2.1 PKA energy

Figure 1 illustrates the schematics of two-body nuclear reactions in the Laboratory (Lab) and the Center of Mass (CM) frames. E and E' respectively denote the kinetic energies of the incident and the emitted particles. E_R refers to the recoil energy of PKA. m and m' respectively represent the masses of the incident and the emitted particles. M and M' respectively denote the masses of the target and the residual particle. In the present work, the incident particle is a neutron. Hence, all masses use the unit of neutron mass. Particularly, one denotes A, a, and A_R for M, m', and M' with the unit of neutron mass.

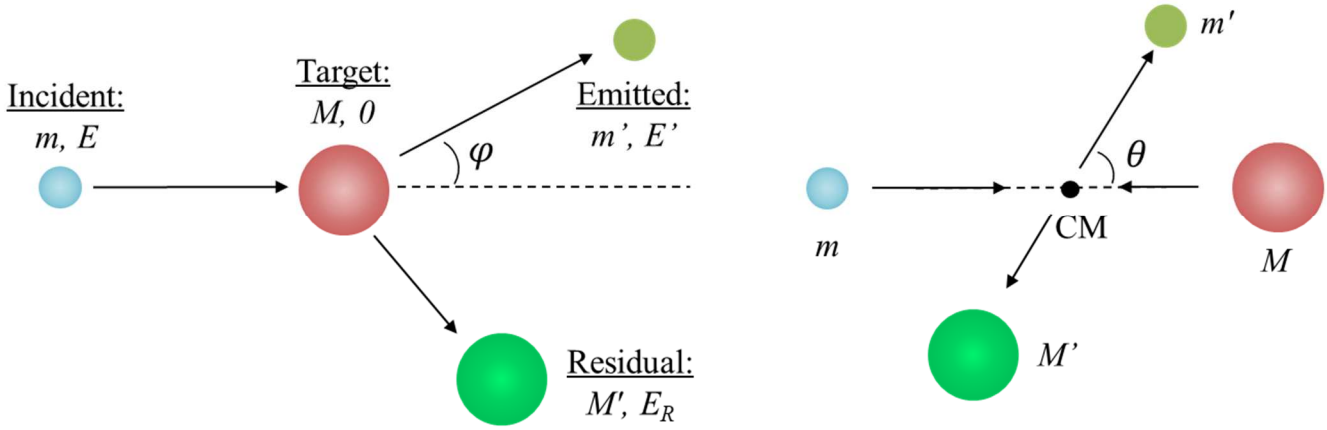

Figure 1. Schematics of the collision in the Laboratory (left) and the Center of Mass (right) frames

Because the relativistic effect is negligible for neutron in fission and fusion reactors [15], the classical mechanical kinematics is used in the present work. For a neutral particle emission, the recoil energy of PKA is [6], [16]:

$$E_R(\mu, E) = \frac{1}{A+1}\left(E^* - 2\sqrt{aE^*E_s}\mu + aE_s\right), \quad (1)$$

where $\mu = \cos\theta$,

$$E^* = \frac{A+1-a}{A+1}E, \quad (2)$$

and

$$E_s = E_a \equiv Q + \frac{A}{A+1}E, \quad (3)$$

where Q is the increase of kinetic energy of the reaction, i.e. decrease of the rest energy minus excitation energy variation. $E^*/(A+1)$ is the kinetic energy of the recoil

nucleus in the CM frame. E_s is the total kinetic energy of the system in the CM frame after the nuclear reaction.

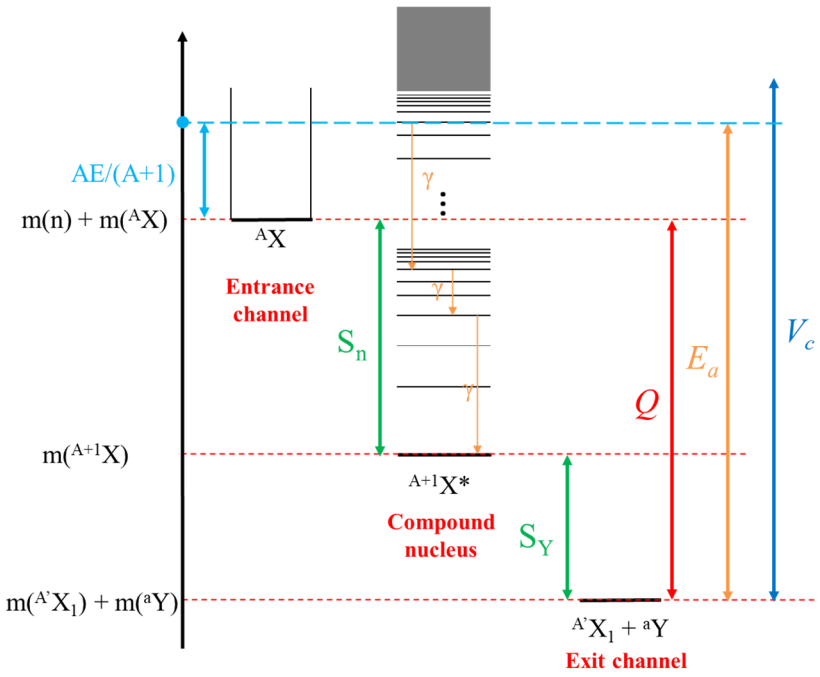

Figure 2. Rest energy of the system: before reaction, in compound nucleus form, and after the nuclear reaction. S_n and S_Y (in green) illustrate the separation energies of neutron and particle ^aY, Q is the mass difference between the entrance channel and the exit channel, V_C is the Coulomb barrier energy.

Figure 2 points out the rest energy of the system from the entrance channel to the exit channel. For two-body charged particle emission nuclear reactions, the system after the collision has the minimum energy that is equal to the Coulomb barrier energy:

$$V_C = k_C \frac{z(Z-z)}{R_0} e^2, \tag{4}$$

where the Coulomb's constant $k_C = 8.988 \times 10^9$ $\mathrm{N \cdot m^2 \cdot C^{-2}}$, the elementary charge $e = 1.60 \times 10^{-19}$ C, z (Z, respectively) is the atomic number of the emitted (target, respectively) nucleus, and the minimum distance among two particles after the collision is

$$R_0 = r_0 a^{1/3} + r_0 (1 + A - a)^{1/3}, \tag{5}$$

where r_0 is about 1.2 to 1.4 fm. For the classical mechanism, if the incident neutron has not enough energy to overcome the Coulomb barrier, i.e. $Q + \frac{A}{A+1}E < V_C$, the reaction cannot happen. However, due to the quantum tunneling, the collision is possible even though $Q + \frac{A}{A+1}E < V_C$. The probability of quantum tunneling is included in the corresponding nuclear reaction cross section. Once the reaction happens, the system has at least the energy of V_C. Therefore, at the end of the acceleration of the emission particle due to the Coulomb force, the recoil energy of

PKA can be calculated using Eq. (1) with

$$E_s = \max(Q + \frac{A}{A+1}E, V_c). \quad (6)$$

For conservative consideration, $r_0 = 1.2$ fm is used to compute the Coulomb barrier. The Coulomb barrier energy is thus numerically calculated by:

$$V_C = \frac{1.198z(Z-z)}{a^{1/3}+(1+A-a)^{1/3}} \text{ MeV}. \quad (7)$$

It is noteworthy that for the numeric application from Eq. (4) to Eq. (7), an elementary charge *e* is kept in the unit MeV.

It is noticeable that the widely used processing code NJOY takes the minimum of $Q + \frac{A}{A+1}E$ and V_C [6]. In the case of $Q + \frac{A}{A+1}E > V_C$, NJOY may consider the energy loss via deexcitation of the compound nucleus. Nevetheless, the formula proposed in the present work can directly imply the formula for neutron scattering reaction [6], [16] using $z = 0$. The Coulomb barrier energy used in NJOY is [6]:

$$V_{C,\text{NJOY}} = \frac{1.029zZ}{a^{1/3}+A^{1/3}} \text{ MeV}. \quad (8)$$

The constant 1.029 is the result of using $r_0 = 1.4$ fm.

2.2 Calculation of DPA cross section in monatomic materials

For a specific PKA energy, the number of DPA can be determined with the methods presented in Section 1. Assuming the relationship between PKA energy and the number of atomic displacements, one can determine the DPA cross section for a given nuclear reaction *i* of the target *j* through:

$$\sigma_{DPA,i,j}(E) = \sigma_{i,j}(E) \int_{-1}^{1} f_{i,j}(\mu, E)\, \nu\big(E_{R,i,j}(\mu, E), i, j\big) d\mu, \quad (9)$$

where $\nu\big(E_{R,i,j}(\mu, E), i, j\big)$ denotes the number of atomic displacements for a PKA energy of $E_{R,i,j}(\mu, E)$, $f_{i,j}(\mu, E)$ is the angular distribution in the CM frame, and $\sigma_{i,j}(E)$ is the reaction cross section. $\nu\big(E_{R,i,j}(\mu, E), i, j\big)$ can be determined with the methods presented in the introduction, such as MD, BCA, and DFT.

The current international standard, also referred to the Norgett-Robinson-Torrens (NRT)-DPA, is [17]:

$$\nu\big(E_{R,i,j}(\mu, E), i, j\big) \equiv \nu\big(T_{a,i,j}\big) = \begin{cases} 0, & T_{a,i,j} < E_{d,j} \\ 1, & E_{d,j} < T_{a,i,j} < 2.5E_{d,j} \\ 0.8T_a/2E_{d,j} & T_{a,i,j} > 2.5E_{d,j} \end{cases} \quad (10)$$

where T_a is the available energy to produce atomic displacement, $E_{d,j}$ is the average threshold energy of atomic displacement. Assuming the utilization of NRT-DPA formula for PKAs of which the atomic number and mass number are close to those of atoms in the lattice, the damage energy is computed with Lindhard's theory [18] and Robinson's analytical fitting [19]:

$$T_{a,i,j}(\varepsilon) = E_{R,i,j}(\mu, E)/[1 + k_L(3.4008\varepsilon^{1/6} + 0.40244\varepsilon^{3/4} + \varepsilon)], \quad (11)$$

where $\varepsilon = E_{R,i,j}(\mu, E)/E_L$, and

$$E_L = \frac{k_C e}{0.8853 a_0} Z_R Z \left(Z_R^{2/3} + Z^{2/3}\right)^{1/2} (A_R + A)/A \ \text{[eV]}, \tag{12}$$

$$k_L = \left(11.53 \frac{m_e}{m_N}\right)^{1/2} \frac{Z_R^{3/3} Z^{1/2} (A_R + A)^{3/2}}{\left(Z_R^{2/3} + Z^{2/3}\right)^{3/4} A_R^{3/2} A^{1/2}}, \tag{13}$$

where Z and A ($Z_R = Z - z$ and $A_R = A + 1 - a$, respectively) are respectively the atomic number and the atomic mass number for lattice atom (PKA, respectively). The other parameters in Eqs. (12) and (13) and the corresponding numerical results for the coefficients in Eqs. (12) and (13) are given in Table 1. We remark that the constant 0.8853 in Eq. (12) is from the screening length $a = 0.8853 a_0 \left(Z_R^{2/3} + Z^{2/3}\right)^{-1/2}$ [18] and the constant 11.53 in Eq. (13) is actually $(2/0.8853)^3$.

Table 1. Constants in Eqs. (12) and (13)

Symbol	k_C	e	a_0	m_e	m_N	$\frac{k_C e}{0.8853 a_0}$	$\left(11.53 \frac{m_e}{m_N}\right)^{1/2}$
Name	Coulomb constant	Elementary charge	Bohr radius	Mass of electron	Mass of nucleon	Coefficient in Eq. (12)	Coefficient in Eq. (13)
Unit	$\mathrm{N \cdot m^2 \cdot C^{-2}}$	C	pm	$\mathrm{MeV/c^2}$	$\mathrm{MeV/c^2}$	-	-
Value	8.988×10^9	1.602×10^{-19}	52.92	0.5110	931.5	30.734	0.07953

The threshold displacement energy is direction-dependent. Due to the use of average threshold energy in NRT-DPA, additional uncertainty of $E_{d,j}$ is introduced in DPA calculations. In order to decrease the influence of $E_{d,j}$ in DPA cross sections calculations, one defines the DPA cross section as the damage energy cross sections by:

$$\sigma_{D,i,j}(E) = \sigma_{i,j}(E) \int_{-1}^{1} f_{i,j}(\mu, E) \left[2.5 E_{d,j} \nu\left(E_{R,i,j}(\mu, E), i, j\right)\right] d\mu. \tag{14}$$

The total damage cross section of atom j is computed by summing all possible reaction channels i:

$$\sigma_{D,j}(E) = \sum_i \sigma_{i,j}(E) \int_{-1}^{1} f_{i,j}(\mu, E) \left[2.5 E_{d,j} \nu\left(E_{R,i,j}(\mu, E), i, j\right)\right] d\mu. \tag{15}$$

The DPA cross sections can be directly deduced by:

$$\sigma_{DPA,j}(E) = \sigma_{D,j}(E) / \left(2.5 E_{d,j}\right). \tag{16}$$

The damage cross section computed by Eq. (15) is not much sensitive to E_d [20], [21] because it depends on $E_{d,j}$ only for $E_{d,j} < T_a < 2.5 E_{d,j}$. Therefore, the advantage is that users can use different threshold energies for computing DPA rates without recalculating the damage cross section Eq. (15). The DPA cross sections calculated in the present work are based on NJOY-2016.20 [22] with the modifications described in Refs. [7], [16] to numerically perform the standard NRT-DPA metric (given in Appendix A1 of this paper). The modifications proposed

in the present work for charged particle emission reactions are: (i) change the Coulomb barrier by Eq. (7) and (ii) change the smaller of available energy and Coulomb barrier by the larger one. The corresponding corrections in the NJOY HEATR module are illustrated in Appendix A2. It should be indicated that isotropic angular distributions in the CM frame are assumed in NJOY for the calculations of damage cross sections induced by charged particle emissions [6], [22].

It is noticeable that Lindhard's theory [18] is valid for PKA energy lower than $24.9A_R Z_R^{4/3}$ keV (or $\varepsilon < 286A/Z$), so is the NRT-DPA formula. This limit of energy is high enough for most isotopes in fission reactors. For example, the upper limits of PKA energies are 107 MeV for ^{56}Fe and 23.5 MeV for ^{28}Si. However, for light PKAs, such as ^{6}Li in fusion reactors and ^{10}B for control systems, the limits are respectively 0.65 MeV and 2.13 MeV, while the maximum PKA energies are much higher than these limits in reactors (c.f. Section 3.1). Therefore, Eq. (10) cannot be used to compute DPA cross sections at high incident energy for light nuclei. For neutron elastic scattering, because the maximum PKA energy is $4EA/(A+1)^2$, the corresponding limit of incident energy is:

$$E_{max} = 6.225Z^{4/3}(A+1)^2 \text{ keV}. \quad (17)$$

2.3 DPA cross section for polyatomic materials

For convenience, let *J* denote polyatomic materials. The damage energy for the polyatomic material *J* is computed by:

$$\sigma_{DPA,J}(E) = \sum_{j\in J} c_j \sum_i \sigma_{i,j}(E) \int_{-1}^{1} f_{i,j}(\mu, E) \left[\nu\left(E_{R,i,j}(\mu, E), i, j, J\right)\right] d\mu, \quad (18)$$

where c_j represents the fraction of atom j in the compound material J, $\nu\left(E_{R,i,j}(\mu, E), i, j, J\right)$ refers to the number of atomic displacements in J by the PKA produced from the reaction i on the target j. Because the NRT-DPA formula is valid only for monatomic materials, the present work uses SRIM/TRIM-2008 [23] for computing displacements in polyatomic materials. This equation can be rewritten as:

$$\sigma_{DPA,J}(E) = \sum_{j\in J} c_j \sum_i \sigma_{i,j}(E) \int_{-1}^{1} f_{i,j}(\mu, E) \left[\nu\left(E_{R,i,j}(\mu, E), i, j\right)\eta(E_R, i, j, J)\right] d\mu, \quad (19)$$

where $\eta(E_R, i, j, J)$ represents the ratio of displacement number in the polyatomic material *J* to that in the monatomic material *j* by the PKA produced by the reaction *i* of atom *j*. The PKA kinetic energy E_R depends on μ. In the case that $\eta(E_R, i, j, J)$ does not depend on E_R nor reaction i, with the notation $\eta(j, J) \equiv \eta(E_R, i, j, J)$, the DPA cross section in compound materials can be expressed by the DPA cross sections in monatomic materials:

$$\sigma_{DPA,J}(E) = \sum_{j\in J} c_j \eta(j, J) \sum_i \sigma_{i,j}(E) \int_{-1}^{1} f_{i,j}(\mu, E) \nu\left(E_{R,i,j}(\mu, E)\right. = \sum_{j\in J} c_j \eta(j, J) \sigma_{DPA,j} \quad (20)$$

Therefore, for $\eta(E_R, i, j, J)$ independent on E_R nor i, the DPA cross sections of polyatomic materials can be directly deduced from the damage energy calculated by

NJOY with:

$$\sigma_{DPA,J}(E) = \sum_{j\in J} c_j \eta(j,J) \sigma_{D,j} / \left(2.5E_{d,j}\right) \quad (21)$$

An important remark is that, due to the different numbers of displacement in *j* and *J*, the computation of total DPA cross section of compound materials with those of elementary atoms is different from the computation for reaction cross sections, which is:

$$\sigma_J(E) = \sum_{j\in J} c_j \sigma_j \quad (22)$$

2.4 Calculation of DPA rate using DPA cross sections

For a specific incident particle, the total DPA rate induced by this particle in material *J* is computed by:

$$\tau_{DPA,J} = \int_0^\infty \sigma_{DPA,J}(E)\phi(E)dE, \quad (23)$$

where $\phi(E)$ represents the spectrum of the incident particle. In practice, the spectra are always given in specific energy grids rather than continuous functions versus energy, two methods are proposed to compute the integral.

In order to directly use the multigroup spectra without introducing additional uncertainties from pointwise interpolation, one can compute the multigroup DPA cross sections. Therefore, the DPA rate is given by:

$$\tau_{DPA,J} = \sum_k \sigma_{DPA,J,k}\phi_k, \quad (24)$$

where the index *k* stands for the group number, the multigroup DPA cross sections being given by the expression:

$$\sigma_{DPA,J,k} = \int_{E_{inf,k}}^{E_{sup,k}} \sigma_{DPA,J}(E)\varphi(E)dE \,/\, \int_{E_{inf,k}}^{E_{sup,k}} \varphi(E)dE, \quad (25)$$

where the weighting function $\varphi(E)$ should be equal to the real continuous spectrum $\phi(E)$ in principal. However, because the real continuous spectrum is unknown, some general functions are proposed. Therefore, additional bias is introduced by multigroup DPA cross sections. An example of reducing this kind of additional bias is shown in our previous work [7].

To avoid the additional bias from multigroup DPA cross sections (especially for highly fluctuating reactions cross sections such as the neutron induced ones), one can use continuous DPA cross sections. However, in this case, the interpolation of incident spectra is required. The advantage of this method is to avoid the calculation of multigroup cross sections on different energy grids. Because the neutron spectra used in the present work are based on different energy structures, this method is applied for DPA rate calculations.

3. Results and discussion

3.1 PKA energies and DPA cross sections

Due to the small contribution of charged particle emission reactions on the total irradiation damage for most nuclei of which the threshold energies of nuclear

reactions are above some keV or MeV, the difference between Eq. (6) and the NJOY-method is negligible for total DPA rate. However, for some nuclei of which charged particle emission channels are open at thermal energy, such as the examples on ^{59}Ni, ^{6}Li, and ^{10}B shown in Figure 3, the differences should be important. Since ^{59}Ni is the product of neutron capture reaction of ^{58}Ni, ^{6}Li is an important source of tritium for D+T fusion reactions, and ^{10}B is an isotope for reactivity control, the numerical results are shown for these isotopes.

Figure 4 shows the maximum PKA energies (i.e. given by Eq. (1) with $\mu = -1$) for 1 MeV, 14.1 MeV, and 20 MeV neutron-induced reactions for ^{10}B and ^{6}Li. 1 MeV is chosen because the conventional measurements of DPA are actually the measurements of neutron fluence above 1 MeV. 14.1 MeV is the energy of D+T fusion produced neutron [24]. 20 MeV is the upper limit of fission reactors. The green lines in Figure 4 are maximum PKA energies of neutron elastic scatterings. They are shown in the figures for comparison. Figure 4 illustrates the large increase in maximum PKA energies if Eq. (6) is used instead of the calculation proposed by NJOY [6]. It is noticeable that the 0 maximum PKA energy of 1 MeV neutron (n,p)-NJOY for ^{6}Li is due to the negative value of $Q + \frac{A}{A+1}E$.

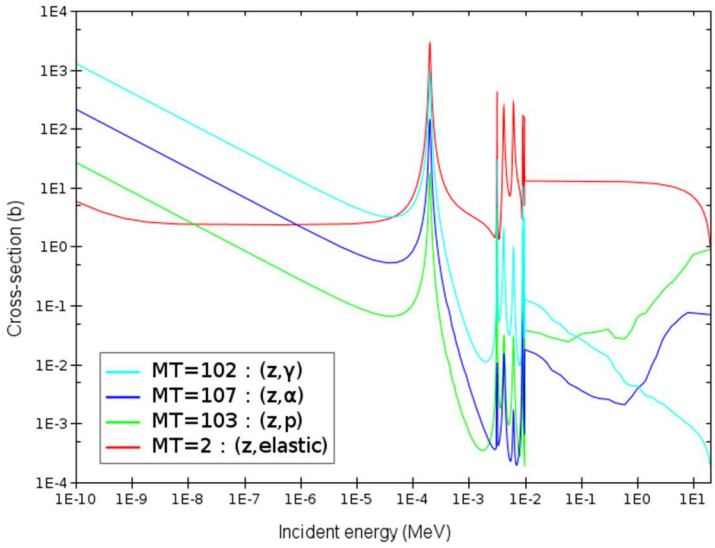

(a)

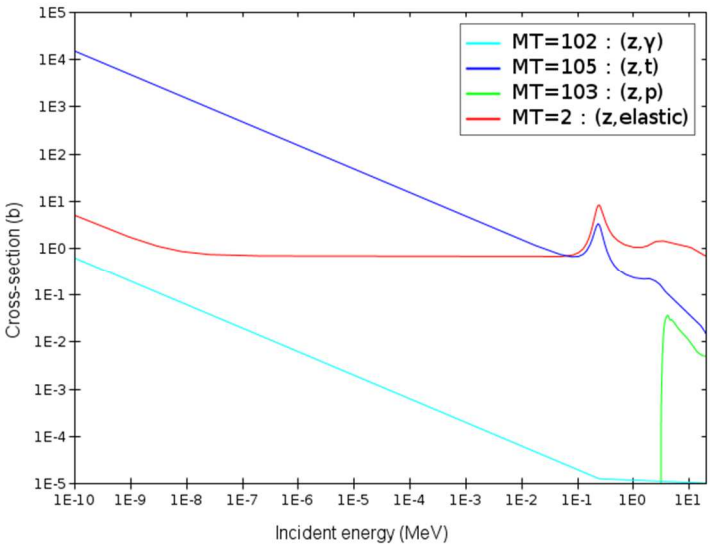

(b)

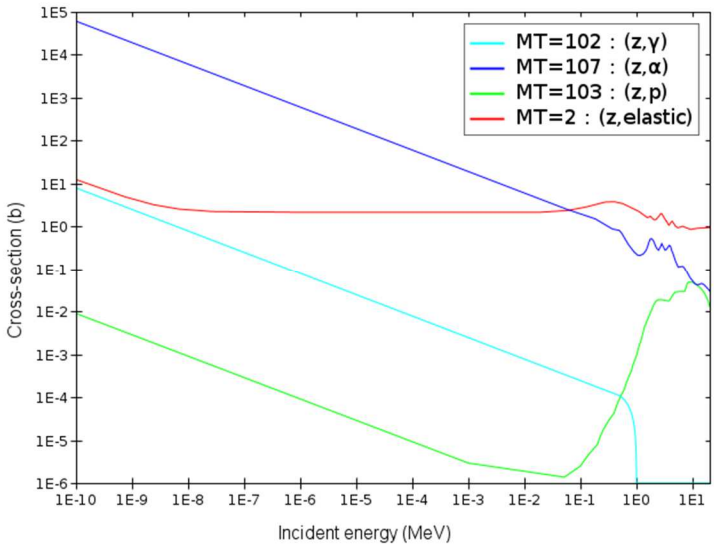

(c)

Figure 3. Reaction cross sections for ^{59}Ni (a), ^{6}Li (b), and ^{10}B (c) from JEFF-3.1.1 [25]

Table 2 summarizes the upper boundary of application for Lindhard's theory [18] presented in Section 2.2 for the reactions shown in Figure 4. The maximum PKA energies shown in Figure 4 are mostly higher or close to the limits pointed out in Table 2. Therefore, Lindhard's theory cannot be directly used, either the NRT-DPA formula. In other words, the NRT formula-based DPA cross sections are not applicable to this kind of cases. Therefore, in order to determine the atomic displacement damage above the limit of Lindhard's theory, the large increase of PKA energies points out the large extension of PKA energy range for computing the DPA cross sections using atomic displacement simulations presented in Section 1.

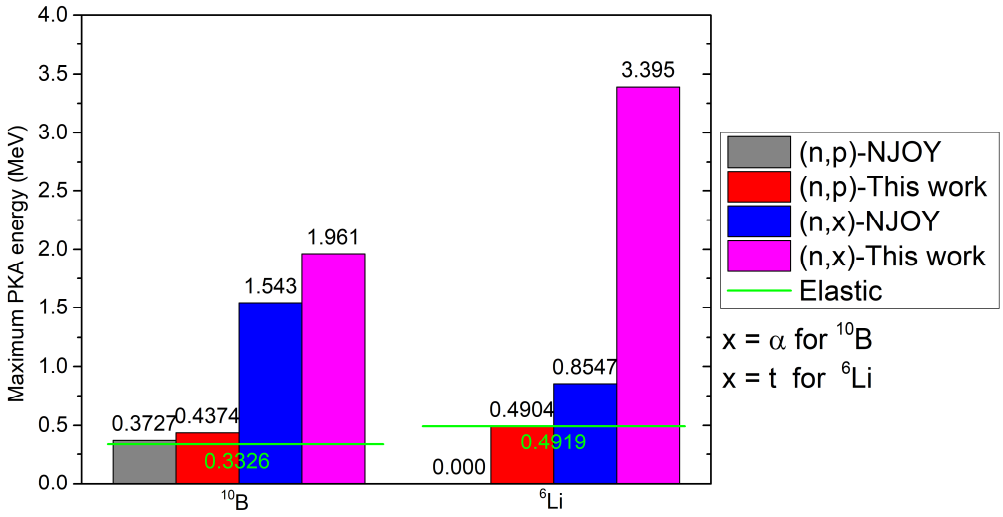

(a)

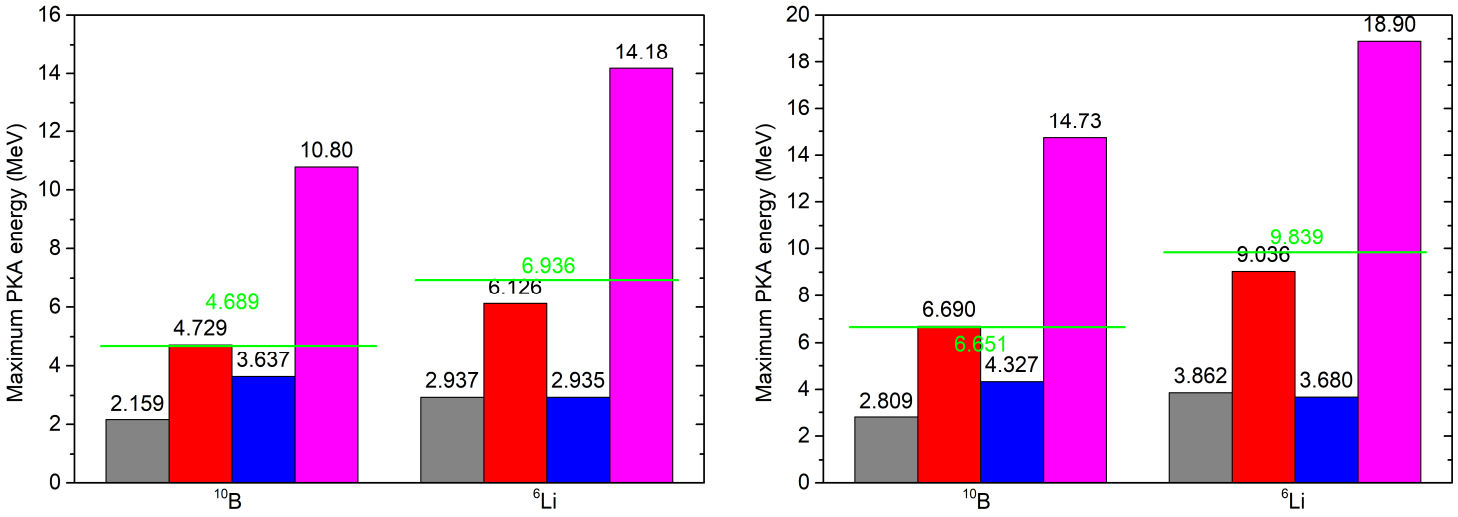

(b) (c)

Figure 4. Maximum PKA energies for 1 MeV (a), 14.1 MeV (b), and 20 MeV (c) neutron-induced reactions for ^{10}B and ^{6}Li. The green lines are maximum PKA energies of neutron elastic scattering.

Table 2. Upper boundaries of PKA energy in Lindhard's theory

Target	Reaction	Z_R	A_R	Limit E_{PKA}(MeV)
^{6}Li	Elastic	3	6	0.646
	(n,p)	2	6	0.376
	(n,t)	2	4	0.251
^{10}B	Elastic	5	10	2.129
	(n,p)	4	10	1.581
	(n,α)	3	7	0.754

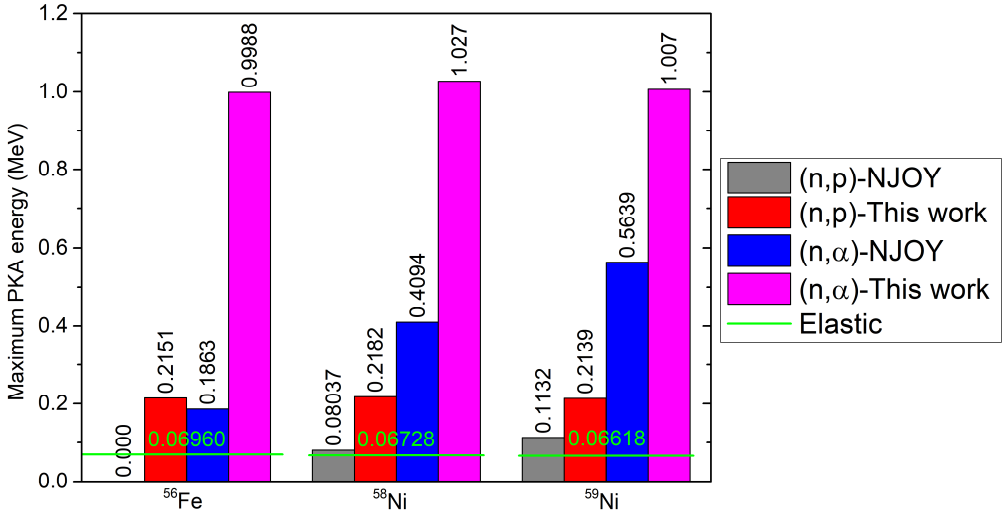

(a)

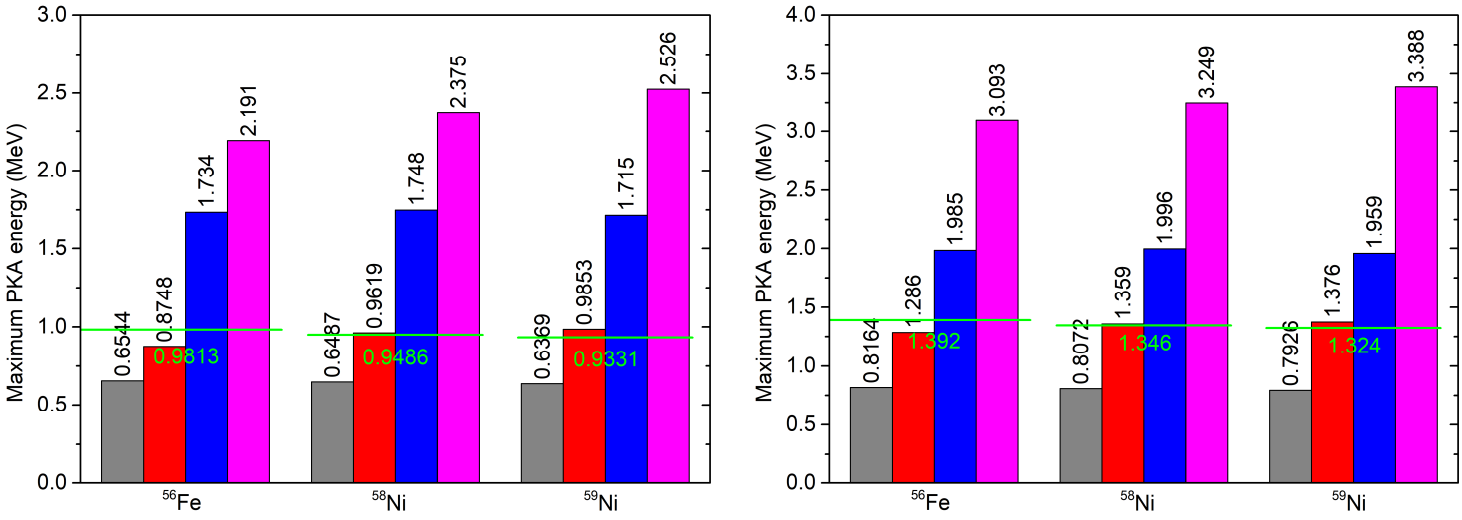

(b) (c)

Figure 5. Maximum PKA energies for 1 MeV (a), 14.1 MeV (b), and 20 MeV (c) neutron-induced reactions for ^{56}Fe, ^{58}Ni, and ^{59}Ni. The green lines are the maximum PKA energies of neutron elastic scattering.

Figure 5 shows similar results as those illustrated in Figure 4 for ^{56}Fe, ^{58}Ni, and ^{59}Ni. Same as the case of ^{6}Li, the 0 maximum PKA energy of 1 MeV neutron (n,p)-NJOY for ^{56}Fe is due to the negative value of $Q + \frac{A}{A+1}E$. For these three isotopes widely used in steel (^{59}Ni is the product of neutron capture reaction of ^{58}Ni), the increase of PKA energies also leads to the extension of energy range for atomic displacement simulations. Nevertheless, because the PKA energies are below the limit of Lindhard's equation for these nuclei, the NRT-DPA formula can be directly applied.

The original NJOY-2016 calculated damage cross sections and the presently proposed calculations are shown in Figure 6 for ^{59}Ni. MT444 is the total damage cross section, MT447 is the sum of damage cross sections induced by reactions without neutron emission. The damage cross sections for disappearance reactions are predominated by the (n,α) reaction for ^{59}Ni [26]. The damage cross section calculated with the methods proposed in the present work is larger than that of NJOY by a factor of 1.8 for neutron energy below 1 keV. The ratio is constant because the recoil energy is approximately proportional to the total kinetic energy of the system in the CM frame, $\max(Q, V_c)$ for the present work and $\min(Q, V_c)$ for NJOY ($Q + \frac{A}{A+1}E \approx Q$ for $Q = 4.88$ MeV [25] and $E < 10$ keV). The difference in total damage cross section is small for energy in the range of [3 MeV, 10 MeV] because the elastic scattering is dominant in this energy range.

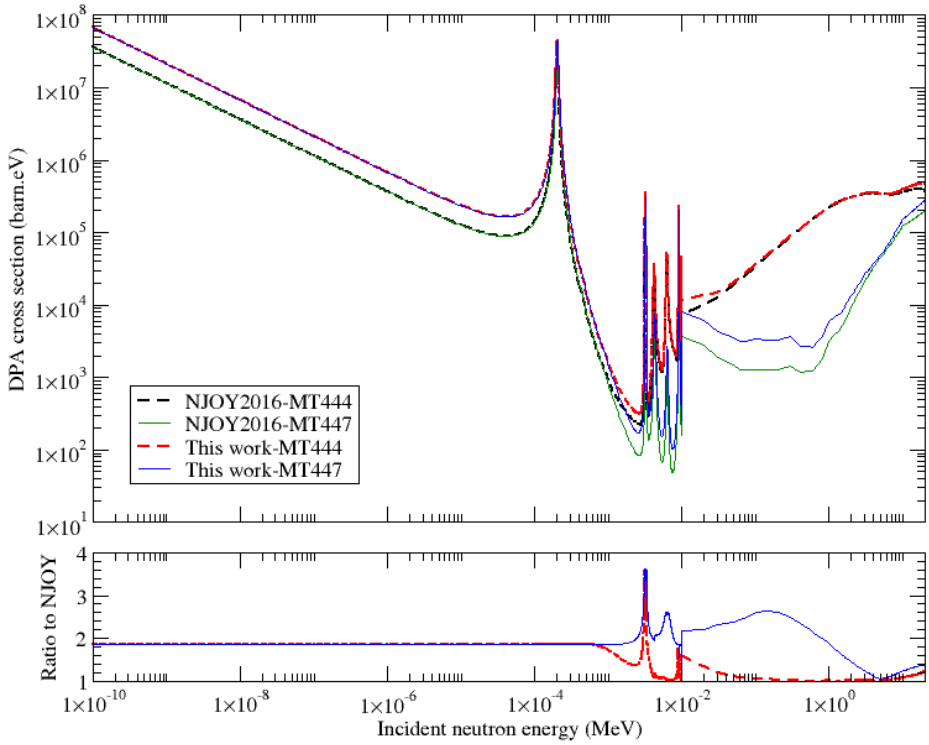

Figure 6. Damage cross sections of ^{59}Ni. MT444 is the total damage cross section, MT447 is the sum of damage cross sections induced by reactions without neutron emission.

It is remarkable that the difference between NJOY and the formula proposed in the present work is important only for reactions starting from thermal energy. The corrections on damage cross sections are not important for most nuclei, such as ^{56}Fe and ^{58}Ni. However, due to the large difference in PKA energies, a large extension of PKA energy range is required if one computes the number of DPA using atomic simulations, such as MD and BCA.

3.2 DPA rates

In order to evaluate the differences in DPA rates using the formula proposed in the present work, neutron flux in different facilities are used. Figure 7 shows the neutron flux determined in the Heavy Reflector (HR) of a Gen-III reactor deduced from the PERLE experiment [27], [28], the inner surface of the Reactor Pressure Vessel (RPV) in a 900 MWe Pressurized Water Reactor (PWR) [16], the fuel cladding in the Sodium-cooled Fast Reactor (SFR) Phenix [16], reflector of ASTRID [7], [29], and a First Mirror Unit (FMU) after the first-wall facing the plasma for a fusion reactor [16]. The corresponding NRT-DPA rates and differences for ^{56}Fe, ^{58}Ni, and ^{59}Ni are tabulated in Table 3. As explained in Section 3.1, the differences for ^{56}Fe, ^{58}Ni are negligible due to the quite small contribution of charged particle emission reactions on the total DPA rate. However, because of its low reaction threshold energies of (n,p) and (n,α) reactions, the differences in total DPA rate for ^{59}Ni are quite important. The largest relative correction is 79% for ^{59}Ni in the inner surface of PWR RPV.

Table 3. DPA rates (in DPA/year) for ^{56}Fe, ^{58}Ni, and ^{59}Ni in different facilities

	Facility	^{56}Fe	^{58}Ni	^{59}Ni
NJOY-2016	Gen-III HR	0.3063	0.4978	3.644
	PWR RPV	0.002866	0.004361	0.1641
	FR Cladding	25.30	42.02	112.2
	ASTRID	0.5679	0.8080	1.161
	Fusion	2.385	3.524	11.33
This work	Gen-III HR	0.3063	0.4978	5.610
	PWR RPV	0.002866	0.004361	0.2942
	FR Cladding	25.30	42.02	117.7
	ASTRID	0.5683	0.8122	1.288
	Fusion	2.386	3.530	15.65
Difference (%)	Gen-III HR	3E-5	2E-4	**54.0**[a]
	PWR RPV	2E-4	0.001	**79.3**
	FR Cladding	4E-5	2E-4	4.8
	ASTRID	0.070	0.52	**10.9**
	Fusion	0.052	0.15	**38.2**

[a] Values in boldface are larger than 10%

Because the materials used in industry are always polyatomic materials rather than pure monatomic materials, the studies on compound materials should be performed. The objective of the present work is to show the change of DPA rates using the total kinetic energy proposed in Section 2.1, the virtual material with 90%Fe and 10%Ni proposed in Ref. [26] is used to simplify the calculations. In addition, because ^{56}Fe has 91.75% abundance in nature iron, the 90%Fe is supposed to be pure ^{56}Fe. Ref. [26] shows the percentage of ^{59}Ni can be about 10% in total nickel. Hence, we suppose 9%^{58}Ni and 1%^{59}Ni for the 10%Ni.

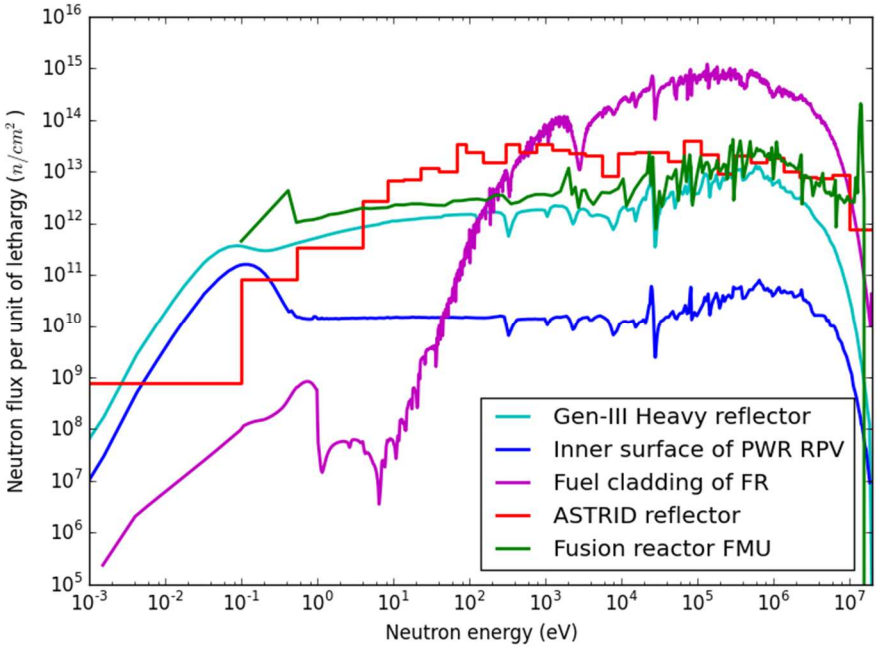

Figure 7. Neutron spectra of different facilities

Because the NRT-DPA formula is not valid for polyatomic materials, the SRIM/TRIM-2008 code [23] is used to determine the number of displacements in the polyatomic material 90%^{56}Fe-9%^{58}Ni-1%^{59}Ni for given PKA energies. Owing to the differences between the numbers of vacancies computed by SRIM and the NRT formula including for monatomic materials [30], [31], the present work performs SRIM simulation for both monatomic materials and the compound material to calculate reasonable values of the ratio $\eta(E_R, i, j, J)$. The use of the ratios deduced from SRIM calculations somewhat avoids the controversy between the quick calculation and the full cascade simulation. Moreover, the obtained results for the polyatomic material, i.e. $\nu(E_R, i, J) = \eta(E_R, i, j, J) \times NRT(E_R, i, j)$, should be coherent with the standard NRT formula. All SRIM simulations are performed with 50 000 incident ions quick calculation without considering binding energies as recommended by Stoller [30]. The threshold displacement energies are 33 eV and 40 eV for Ni and Fe, respectively [4], [32]. The results of SRIM simulations and the deduced values of $\eta(E_R, i, j, J)$are shown in Figure 8. Only the ratios $\eta(E_R, i, j, J)$ are used in the following studies.

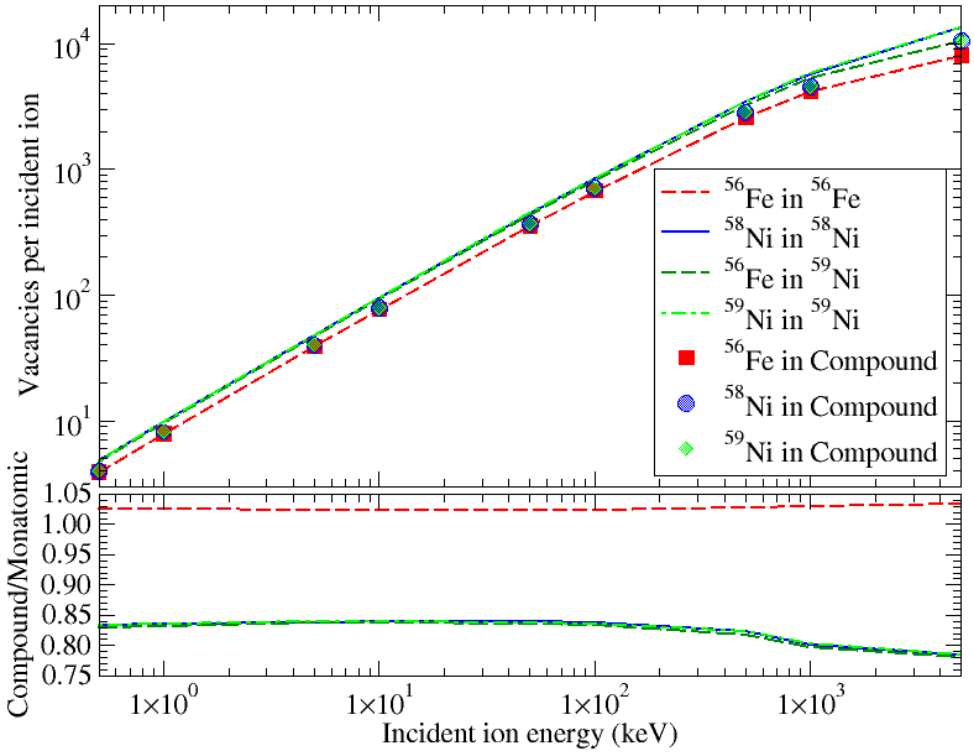

Figure 8. Number of vacancies in monatomic materials and the compound material 90%^{56}Fe-9%^{58}Ni-1%^{59}Ni computed by SRIM-2008 quick calculation. The lower plot shows the ratios of vacancies in the compound material to those in the monatomic materials.

Figure 8 shows that the ratio of vacancies in the considered compound material to those in pure monatomic materials is almost constant for a specific iron. The values different to the unity are due to the different electronic stopping powers and the different threshold energies. For compound materials, the equivalent threshold displacement energy can be calculated by [33]:

$$E_{d,eq} = \left(\sum_j c_j / E_{d,j}\right)^{-1}, \tag{26}$$

where c_j and $E_{d,j}$ are respectively the relative atomic concentration and the threshold displacement energy of the atom j. This equation is validated by $MgA1_2O_4$ via binary collision Monte Carlo simulations [33]. Using Eq. (26), the equivalent threshold energy for the compound material 90%^{56}Fe-9%^{58}Ni-1%^{59}Ni is 39.2 eV. The NRT-DPA formula points out that the DPA is inversely proportional to the displacement threshold energy. Therefore, the 39.2 eV equivalent threshold energy leads to the ratios of 1.02 and 0.84 for DPA induced by a specific PKA in the compound material to the ones in the iron and nickel monatomic materials, respectively. The ratios shown in Figure 8 are close to these values simply deduced by different threshold energies. Therefore, in SRIM quick calculation module, the atomic displacement threshold energy plays the predominant role in the correction of atomic displacement in the polyatomic material 90%Fe-10%Ni.

Because Figure 8 points out that the ratios $\eta(E_R, i, j, J)$ are weakly dependent on

PKA energy for the three PKAs in iron or nickel to those in the compound material 90%^{56}Fe-9%^{58}Ni-1%^{59}Ni, Eq. (20) can give a good approximation for the total DPA cross section of 90%^{56}Fe-9%^{58}Ni-1%^{59}Ni:

$$\sigma_{DPA,J}(E) = 0.9 \times 1.02\sigma_{DPA,^{56}\mathrm{Fe}} + 0.09 \times 0.84\sigma_{DPA,^{58}\mathrm{Ni}} + 0.01 \times 0.84\sigma_{DPA,^{59}\mathrm{Ni}} \quad (27)$$

Because the given neutron flux is independent on the nuclei, the total DPA rate in the compound 90%^{56}Fe-9%^{58}Ni-1%^{59}Ni is:

$$\tau_{DPA,J}(E) = 0.918\tau_{DPA,^{56}\mathrm{Fe}} + 0.0756\tau_{DPA,^{58}\mathrm{Ni}} + 0.0084\tau_{DPA,^{59}\mathrm{Ni}} \quad (28)$$

Table 4. DPA rates (in DPA/year) for 90%^{56}Fe-9%^{58}Ni-1%^{59}Ni in different nuclear facilities calculated via Eq. (28)

	Gen-III HR	PWR RPV	FR Fuel	ASTRID	Fusion
NJOY-2016	0.3494	0.004318	27.30	0.5913	2.551
This work	0.3660	0.005398	27.34	0.5931	2.589
Difference	4.73%	25.0%	0.16%	0.29%	1.48%

The DPA rates in different nuclear facilities computed by Eq. (28) are given in Table 4. The difference between the two methods is 25% for the flux at the inner surface of PWR RPV, while the values are about 5% for the heavy reflector and fusion first wall. The difference is negligible for two fast neutron flux. Because the differences are negligible for ^{56}Fe and ^{58}Ni (shown in Table 3), the differences in DPA rates in the compound material are directly determined by the percentage of DPA induced by neutron reactions with ^{59}Ni. Figure 6 and Figure 9 (in Appendix A3) show that the damage cross sections of ^{59}Ni are much larger than those of ^{56}Fe and ^{58}Ni for incident neutron energy below 600 eV. Therefore, for the nuclear facilities having a higher proportion of neutron with energies below 600 eV, the differences in total DPA rates calculated with the two methods of PKA energy are larger. This conclusion can be confirmed with data shown in Figure 7 and Table 4.

4. Conclusions

The present work proposes the calculation of PKA energy for charged particle emission nuclear reactions by taking the quantum tunneling effect and the Coulomb barrier into account. Compared with the method used in NJOY [6], large increases of PKA energies are observed for charged particle emission reactions. For instance, for a 14.1 MeV incident neutron, the maximum PKA energies are increased from 2.9 MeV to 14.2 MeV for the ^{6}Li(n,t)^{4}He PKA. Therefore, large difference will be found between the two methods for D+T fusion reactors, of which the 14.1 MeV neutron is the product of D+T fusion and ^{6}Li is an important source of tritium. The proposed method is now implemented in CONRAD for irradiation damage calculation [21].

For most isotopes that the DPA is predominated by neutron scattering reactions, the two different methods for computing the recoil energy of charged particle emission reactions have a limited influence on the total DPA rate, such as for ^{56}Fe and

^{58}Ni. However, the difference is quite important for charged particle emission channels open at thermal energy, such as ^{6}Li, ^{10}B, and ^{59}Ni. The differences of total DPA rates are within 1% for ^{56}Fe and ^{58}Ni in the heavy reflector, RPV of PWR, fuel cladding and reflector of SFR, and fusion first wall, while the corresponding differences are from 5% up to 79% for ^{59}Ni. It is noticeable that the difference of the DPA rate for ^{6}Li and ^{10}B is not calculated because the maximum PKA energies are higher than the upper limit of application for the Lindhard equation governing irradiation damage [18].

The SRIM/TRIM-2008 [23] Monte Carlo simulations show that the ratios number of vacancies produced by main PKAs in 90%^{56}Fe-9%^{58}Ni-1%^{59}Ni to the ones in monatomic materials almost depend only on the equivalent threshold displacement energy in the lattice. Therefore, Eq. (20) proposed in the present work can be applied for the polyatomic material 90%^{56}Fe-9%^{58}Ni-1%^{59}Ni. The DPA cross sections of this compound material can be thus simply deduced from those of ^{56}Fe, ^{58}Ni, and ^{59}Ni.

In order to evaluate the difference of total DPA rate in compound materials, the calculations on the polyatomic material 90%^{56}Fe-9%^{58}Ni-1%^{59}Ni are performed. The relative differences in total DPA rates are within 1% for two fast spectra, 1.5% for fusion first wall, about 5% for the heavy reflector, and 25% for the PWR RPV inner surface. Therefore, the two different methods can have a large difference in total DPA rate for materials containing isotopes of which some charged particle emission channels open at thermal energy.

Acknowledgments

The authors acknowledge Dr. Olivier Serot for useful discussions on the calculation of recoil energy for charged particle emission reaction. Special thanks to our colleagues Dr. Yannick Peneliau, Dr. Laurent Buiron, and Dr. Stéphane Bourganel for providing neutron spectra.

Appendix

A1. Adding one atomic displacement for damage energy in the range of [E_d, 2.5E_d] in the NJOY-2016.20 HEATR module (in red) [16]

```
else if (e.lt.break) then
      df=0
else if (e.lt.2*break/0.8) then
      df=2*break/0.8
else
      ep=e*rel
      dam=e/(1+fl*(c3*ep**sixth+c4*ep**threeq+ep))
      df=dam
endif
```

A2. Changing the damage cross sections for charged particle emission reactions (changes are shown in red)

Original:

```
real(kr),parameter::econ=1.029e6_kr
…
if (ax.ne.zero) denom=1/(ax**third+awr**third)
…
ec=econ*zx*z*denom
ea=q+awr*e*aw1fac
if (ea.ge.zero) then
      et=(awr+1-ax)*e*aw1fac
      if (ea.gt.ec*(1+eps)) ea=ec
      do iq=1,nq
            er=(et-2*sqrt(et*ax*ea)*qp(iq)+ax*ea)*aw1fac
            dame=dame+qw(iq)*df(er,z-zx,awr+1-ax,z,awr)/2
      enddo
endif
```

Changed:

```
real(kr),parameter::econ=1.198e6_kr
…
if (ax.ne.zero) denom=1/(ax**third+(awr+1-ax)**third)
…
ec=econ*zx*(z-zx)*denom
ea=q+awr*e*aw1fac
et=(awr+1-ax)*e*aw1fac
if (ea.lt.ec*(1-eps)) ea=ec
do iq=1,nq
      er=(et-2*sqrt(et*ax*ea)*qp(iq)+ax*ea)*aw1fac
      dame=dame+qw(iq)*df(er,z-zx,awr+1-ax,z,awr)/2
enddo
```

A3: Additional damage cross sections

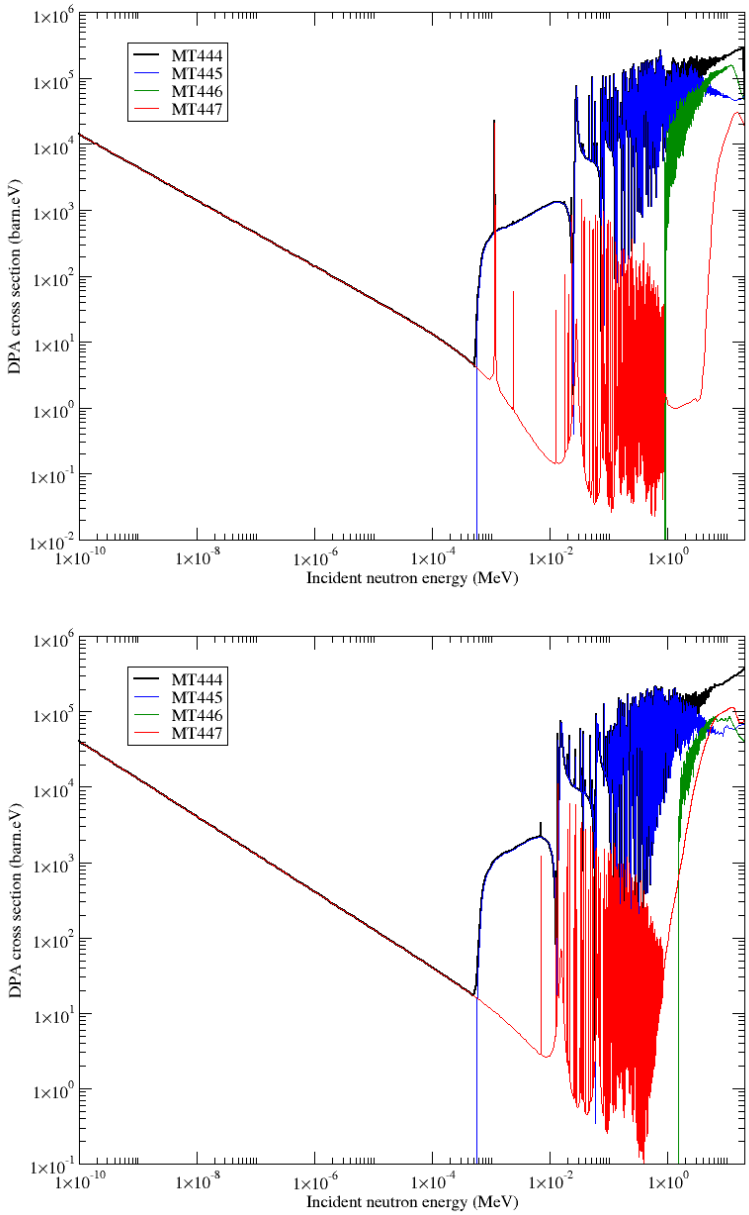

Figure 9. Neutron irradiation damage cross sections for ^{56}Fe (upper) and ^{58}Ni (lower) calculated with modified NJOY-2016.20. MT445 and MT446 respectively represent the damage cross sections for elastic and inelastic neutron scatterings.

References

[1] M. T. Robinson and I. M. Torrens, "Computer simulation of atomic-displacement cascades in solids in the binary-collision approximation," *Phys. Rev. B*, vol. 9, no. 12, pp. 5008–5024, Jun. 1974, doi: 10.1103/PhysRevB.9.5008.

[2] J. B. Gibson, A. N. Goland, M. Milgram, and G. H. Vineyard, "Dynamics of Radiation Damage," *Phys. Rev.*, vol. 120, no. 4, pp. 1229–1253, Nov. 1960, doi: 10.1103/PhysRev.120.1229.

[3] F. Seitz, "On the disordering of solids by action of fast massive particles,"

Discuss. Faraday Soc., vol. 5, pp. 271–282, 1949.

[4] K. Nordlund *et al.*, "Primary Radiation Damage in Materials," OECD/NEA Working Party on Multiscale Modelling of Fuels and Structural Materials for Nuclear Systems, Expert Group on Primary Radiation Damage Nuclear Science, NEA/NSC/DOC(2015)9, 2015. [Online]. Available: https://www.oecd-nea.org/science/docs/2015/nsc-doc2015-9.pdf.

[5] C. S. Becquart, A. De Backer, and C. Domain, "Atomistic Modeling of Radiation Damage in Metallic Alloys," in *Handbook of Mechanics of Materials*, S. Schmauder, C.-S. Chen, K. K. Chawla, N. Chawla, W. Chen, and Y. Kagawa, Eds. Singapore: Springer Singapore, 2018, pp. 1–30.

[6] R. E. MacFarlane, D. W. Muir, and F. M. Mann, "Radiation Damage Calculations with NJOY," *J. Nucl. Mater.*, vol. 123, no. 1–3, pp. 1041–1046, 1984, doi: https://doi.org/10.1016/0022-3115(84)90216-2.

[7] S. Chen, D. Bernard, and L. Buiron, "Study on the self-shielding and temperature influences on the neutron irradiation damage calculations in reactors," *Nucl. Eng. Des.*, vol. 346, pp. 85–96, May 2019, doi: 10.1016/j.nucengdes.2019.03.006.

[8] S. Chen, D. Bernard, and C. De Saint Jean, "Calculation and analysis of gamma-induced irradiation damage cross section," *Nucl. Instrum. Methods Phys. Res. Sect. B Beam Interact. Mater. At.*, vol. 447, pp. 8–21, May 2019, doi: 10.1016/j.nimb.2019.03.035.

[9] A. Yu. Konobeyev, U. Fischer, and S. P. Simakov, "Improved atomic displacement cross-sections for proton irradiation of aluminium, iron, copper, and tungsten at energies up to 10 GeV," *Nucl. Instrum. Methods Phys. Res. Sect. B Beam Interact. Mater. At.*, vol. 431, pp. 55–58, Sep. 2018, doi: 10.1016/j.nimb.2018.06.021.

[10] Y. Iwamoto *et al.*, "Measurement of displacement cross sections of aluminum and copper at 5 K by using 200 MeV protons," *J. Nucl. Mater.*, vol. 508, pp. 195–202, Sep. 2018, doi: 10.1016/j.jnucmat.2018.05.038.

[11] Y. Iwamoto, H. Iwamoto, M. Harada, and K. Niita, "Calculation of displacement cross-sections for structural materials in accelerators using PHITS event generator and its applications to radiation damage," *J. Nucl. Sci. Technol.*, vol. 51, no. 1, pp. 98–107, Jan. 2014, doi: 10.1080/00223131.2013.851042.

[12] S. Chen and D. Bernard, "On the beta decay-induced radiation damage," *Nucl. Instrum. Methods Phys. Res. Sect. B Beam Interact. Mater. At.*, vol. 467, pp. 58–64, Mar. 2020, doi: 10.1016/j.nimb.2020.01.017.

[13] NEA, "JEFF-3.3 Nuclear Data library," http://www.oecd-nea.org/dbdata/JEFF33, Nov. 2017.

[14] D. Gosset, P. Herter, and V. Motte, "Evaluation of damage in neutron irradiated boron carbide," *Nucl. Instrum. Methods Phys. Res. Sect. B Beam Interact. Mater. At.*, vol. 434, pp. 66–72, Nov. 2018, doi: 10.1016/j.nimb.2018.08.021.

[15] S. Chen and D. Bernard, "Relativistic effect on two-body reaction inducing atomic displacement," *J. Nucl. Mater.*, vol. 522, pp. 236–245, Aug. 2019, doi: 10.1016/j.jnucmat.2019.05.020.

[16] S. Chen *et al.*, "Calculation and verification of neutron irradiation damage with differential cross sections," *Nucl. Instrum. Methods Phys. Res. Sect. B Beam Interact. Mater. At.*, vol. 456, pp. 120–132, Oct. 2019, doi: 10.1016/j.nimb.2019.07.011.

[17] M. J. Norgett, M. T. Robinson, and I. M. Torrens, "A proposed method of calculating displacement dose rates," *Nucl. Eng. Des.*, vol. 33, no. 1, pp. 50–54, Aug. 1975, doi: 10.1016/0029-5493(75)90035-7.

[18] J. Lindhard, V. Nielsen, M. Scharff, and P. V. Thomsen, "Integral equations governing radiation effects," *Mat Fys Medd Dan Vid Selsk*, vol. 33, no. 10, pp. 1–42, 1963.

[19] M. T. Robinson, "Energy Dependence of Neutron Radiation Damage in Solids," *Nucl. Fusion React.*, pp. 364–378, 1970.

[20] D. Bernard, "Estimation of bias and uncertainties for radiation damage calculation (Fission Reactors)," IAEA INDC International Nuclear Data Committee, Nuclear Reaction Data and Uncertainties for Radiation Damage, INDC(NDS)-0719, 2016. [Online]. Available: https://uu.diva-portal.org/smash/get/diva2:955795/FULLTEXT01.pdf.

[21] S. Chen, P. Tamagno, D. Bernard, P. Archier, and G. Noguere, "From nuclear physics to displacement damage calculation and uncertainty propagation in CONRAD," *Results Phys.*, vol. 17, p. 103023, Jun. 2020, doi: 10.1016/j.rinp.2020.103023.

[22] R. E. MacFarlane, D. W. Muir, R. M. Boicourt, A. C. Kahler, and J. L. Conlin, "The NJOY Nuclear Data Processing System, Version 2016," Los Alamos National Laboratory (LANL), Los Alamos, NM, United States, LA-UR-17-20093, 2016.

[23] J. F. Ziegler, M. D. Ziegler, and J. P. Biersack, "SRIM – The stopping and range of ions in matter (2010)," *Nucl. Instrum. Methods Phys. Res. Sect. B Beam Interact. Mater. At.*, vol. 268, no. 11, pp. 1818–1823, Jun. 2010, doi: 10.1016/j.nimb.2010.02.091.

[24] J. Knaster, A. Moeslang, and T. Muroga, "Materials research for fusion," *Nat. Phys.*, pp. 424–434, May 2016, doi: 10.1038/nphys3735.

[25] A. Santamarina *et al.*, "The JEFF-3.1.1 Nuclear Data Library," OECD/NEA, JEFF Report 22, NEA No. 6807, 2009.

[26] L. Lunéville, J. C. Sublet, and D. Simeone, "Impact of nuclear transmutations on the primary damage production: The example of Ni based steels," *J. Nucl. Mater.*, vol. 505, pp. 262–266, Jul. 2018, doi: 10.1016/j.jnucmat.2017.06.039.

[27] C. Vaglio-Gaudard *et al.*, "Interpretation of PERLE Experiment for the Validation of Iron Nuclear Data Using Monte Carlo Calculations," *Nucl. Sci. Eng.*, vol. 166, no. 2, pp. 89–106, Oct. 2010, doi: 10.13182/NSE09-91.

[28] S. Chen and D. Bernard, "Attenuation of atomic displacement damage in the heavy reflector of the PERLE experiment and application to EPR," *Nucl. Eng. Des.*, vol. 353, p. 110205, Nov. 2019, doi: 10.1016/j.nucengdes.2019.110205.

[29] T. Beck *et al.*, "Conceptual design of ASTRID radial shielding sub-assemblies," *Nucl. Eng. Des.*, vol. 330, pp. 129–137, Apr. 2018, doi:

10.1016/j.nucengdes.2018.01.040.

[30] R. E. Stoller, M. B. Toloczko, G. S. Was, A. G. Certain, S. Dwaraknath, and F. A. Garner, "On the use of SRIM for computing radiation damage exposure," *Nucl. Instrum. Methods Phys. Res. Sect. B Beam Interact. Mater. At.*, vol. 310, pp. 75–80, Sep. 2013, doi: 10.1016/j.nimb.2013.05.008.

[31] S. Chen and D. Bernard, "On the calculation of atomic displacements using damage energy," *Results Phys.*, vol. 16, p. 102835, Mar. 2020, doi: 10.1016/j.rinp.2019.102835.

[32] C. H. M. Broeders and A. Yu. Konobeyev, "Defect production efficiency in metals under neutron irradiation," *J. Nucl. Mater.*, vol. 328, no. 2, pp. 197–214, Jul. 2004, doi: 10.1016/j.jnucmat.2004.05.002.

[33] N. M. Ghoniem and S. P. Chou, "Binary collision Monte Carlo simulations of cascades in polyatomic ceramics," *J. Nucl. Mater.*, vol. 155–157, no. Part 2, pp. 1263–1267, Jul. 1988, doi: 10.1016/0022-3115(88)90508-9.